

Boolean chaos in one dimension

Seth D. Cohen

Miltec Corp., A Ducommun Company, 678 Discovery Drive, Huntsville, Alabama 35806 USA

(Dated: February 13, 2022)

We demonstrate an experimental realization of one-dimensional chaos in an autonomous Boolean network. The network outputs an unclocked pulse-train of Boolean states, where the widths of sequential pulses are characterized by a simple return map. The system is designed with separate pulse-width stretching and folding functions to realize a map operator consisting entirely of asynchronous logic gates. The operator's output is fed back to its input to continuously iterate the map. The resulting dynamics are similar to that of a tent map with scale-dependent features that arise due to the discrete nature of the system's logic gates.

PACS numbers: 05.45.-a, 05.45.Ac, 05.45.Gg, 84.30.Ng

Boolean chaos is a term used to describe the phenomenon of deterministic dynamics in unclocked Boolean networks with an exponential divergence of neighboring trajectories. Originally, theories of continuous, ideal Boolean networks predicted non-repeating switching in certain networks, but without chaos [1]. Contrary to this prediction, recent experiments demonstrated that analog effects in digital logic gates can introduce non-ideal behaviors that give rise to such Boolean chaos [2]. Boolean chaos has been reported in both autonomous and driven networks [2, 3], both of which yield complex, multi-dimensional dynamics. One-dimensional (1D) Boolean chaos is theorized for specific non-ideal effects [4], but experimental realizations have yet to be found until now.

The simplicity of 1D Boolean chaos makes it an ideal candidate for improving our understanding of Boolean chaotic systems. High-dimensional chaos (Boolean or otherwise) typically requires numerical approaches in its analysis [2], whereas 1D chaos can be examined with analytic techniques. As examples, the derivatives of 1D chaotic return maps yield simple Lyapunov exponent calculations [5], and 1D maps can provide a readily available symbolic dynamics [6] and aid in entropy calculations [7]. Thus, applications of 1D Boolean chaos include simple entropy sources for random number generators [8].

In addition to previous works on Boolean chaos, our research is influenced by recent studies of low-dimensional, non-chaotic dynamics in autonomous Boolean systems. In particular, networks of logic gates that transmit and receive pulses in an autonomous fashion were studied as excitable systems with synchronization patterns [9, 10]. Experiments have also demonstrated Boolean phase oscillators that can exhibit chimera states [11, 12]. One appealing feature of these Boolean systems is that they can be implemented entirely on a field-programmable gate array (FPGA), a common component in modern electronics. This flexible platform allows a user to easily create large dynamical networks of asynchronous logic gates well beyond what can be implemented using discrete components [8–12]. The implementation of our experiment is also facilitated by an FPGA, and the result-

ing 1D Boolean chaos is thus easily transferrable into existing systems with such digital hardware.

In this article, we present a 1D chaotic map with dynamics in the switching times of discrete logic states such that the widths of output pulses are the state variables of the chaos. Shown in Fig. 1a, we design an experiment that is initiated with input pulse v_0 of initial pulse-width w_0 . This pulse drives a map operator M which consists of two separate functions: a piecewise-linear, pulse-width folding-function f and a pulse-width gain-function g that approximately doubles a pulse's width. The output voltage of M is labeled as v_{out} , and a continuous delay line τ_N routes v_{out} back to the input of M , where τ_N is long enough to ensure only one pulse is in this feedback loop at a time so that pulses do not interact. This system remains in a stable steady state $v_{out} = 0$ V until we inject v_0 , and thus w_0 serves as its initial condition.

After v_0 is injected, the map iterates autonomously, creating a self-sustaining pulse-train with varying widths.

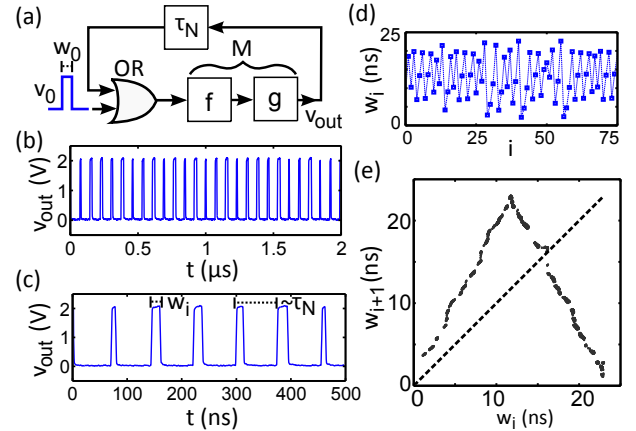


FIG. 1. (a) Experimental system with operator M , initial pulse v_0 injected via OR gate, output voltage v_{out} , and feedback loop of delay $\tau_N \sim 60$ ns (realized using $N = 200$ NOT gates) implemented on an Altera Cyclone IV FPGA (EP4CE115F29C7N) using $\sim 1\%$ FPGA resources. (b)-(c) v_{out} from $w_0 = 16$ ns. (d) w_i as a function of iteration i . (e) Return map (w_i, w_{i+1}) with dashed line of slope 1.

In Figs. 1b-c, we plot the temporal evolution of v_{out} . In the figure, v_{out} contains pulses that occur with spacing $\sim \tau_N$ and aperiodic pulse-widths w_i shown in Fig. 1d. To construct a return map, we plot consecutive widths (w_i, w_{i+1}) in Fig. 1e, which shows that a large portion of a 1D structure is visible with features similar to that of a tent map [5]. This is an indicator of chaos, which we confirm later by calculating the Lyapunov exponent of the return map's dynamics. In the remainder of this paper, we first outline the map operator's functions and then analyze the features of the resulting chaos.

The folding function f is implemented using the circuit shown in Fig. 2. Its design exploits the propagation delays of pulses as they transmit through logic gates. Shown in Fig. 2a, a delay line is constructed using cascaded NOT gates [9], where even numbers of NOT gates are used to reduce asymmetries between rise and fall times of pulse edges that propagate [2] and preserve pulse widths. The number of NOT gates n sets the propagation delay τ_n from input to output.

The input and output of the folding circuit are pulses v_{in} and v_{out} of pulse-widths w_{in} and w_{out} , respectively. As shown in Fig. 2b, v_{in} drives one input of two AND gates, where it is inverted at the input of AND-gate₂. In this circuit topology, a delayed version of the output from AND-gate₁ drives their second inputs, where the delayed feedback of AND-gate₁ is inverted. The resulting output of AND-gate₁ is a pulse of width w_{in} for $w_{\text{in}} \leq \tau_n$. For $\tau_n < w_{\text{in}} \leq 2\tau_n$, the output of AND-gate₁ is a pulse with fixed width $\sim \tau_n$. Because AND-gate₂ receives an inverted version of v_{in} , $v_{\text{out}} = 0$ for the duration of v_{in} , and thus for $\tau_n < w_{\text{in}} \leq 2\tau_n$, $w_{\text{out}} \sim (2\tau_n - w_{\text{in}})$.

To illustrate this circuit's folding, in Fig. 2c we plot experimental examples of $(v_{\text{in}}, v_{\text{out}})$ of the folding circuit, and in Fig. 2d, we scan w_{in} and plot the respective w_{out} . We note that the domain of w_{in} for which $w_{\text{out}} > 0$ is $w_{\text{in}} \in [w_{\text{in,min}} = 4.9 \text{ ns}, w_{\text{in,max}} = 22.6 \text{ ns}]$. Nevertheless, the folding can be approximated as the function

$$f(w_{\text{in}}) = w_{\text{out}} \sim \begin{cases} mw_{\text{in}}, & w_{\text{in}} \leq \tau_n \\ m(2\tau_n - w_{\text{in}}), & \tau_n < w_{\text{in}} \leq 2\tau_n \end{cases} \quad (1)$$

where $m \sim 1$ in Fig. 2d. Thus, this circuit maps w_{in} to w_{out} through a piecewise-linear folding function.

The pulse-width gain circuit also uses a delay line of logic gates and is shown Fig. 3a. In the figure, an input pulse v_{in} is launched into a chain of NOT gates, where AND gates monitor the outputs of gates $(k, 2k)$, where k is the index number of K total NOT gates such that $2k_{\text{max}} = K$. The AND-gate outputs drive a multi-input OR-gate, which outputs a pulse v_{out} with width $w_{\text{out}} \sim 2w_{\text{in}}$ for $\tau_K > w_{\text{out}}$, where τ_K is the delay through K gates. To illustrate the pulse-width gain from this circuit, we plot examples of $(v_{\text{in}}, v_{\text{out}})$ and a scan of $(w_{\text{in}}, w_{\text{out}})$ in Figs. 3b-c, respectively. The resulting waveforms show approximate pulse-width doubling and the characterization of $(w_{\text{in}}, w_{\text{out}})$ shows an average slope

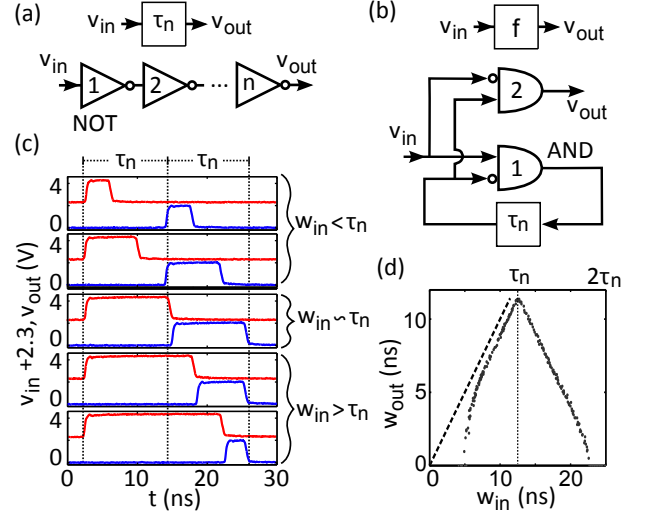


FIG. 2. Pulse-width folding circuit. (a) Delay $\tau_n \sim n \cdot 0.3 \text{ ns}$ comprised of NOT gates (similar to Ref. [9]). (b) f with τ_n for $n = 40$ and AND gates to map v_{in} to v_{out} . (c) v_{in} (top) and v_{out} (bottom) using a Tektronix TDS7254B digital oscilloscope and Hewley Packard Pulse Generator (PG) 8116A. A buffer gate at the input of f removes analog characteristics from the PG. (d) w_{out} for values of w_{in} in 100 ps steps and dashed line of slope 1. We note the folding repeats every $2\tau_n$.

~ 2 for $w_{\text{in}} > 6 \text{ ns}$. Thus, this circuit's function can be approximated as a linear gain $g(w_{\text{in}}) = 2w_{\text{in}}$.

The setup of this pulse-width gain circuit is unconventional, and to help explain its results, we outline the underlying physics of its design. In Fig. 4a, we calculate the overlap R of two identical pulses v_1 and v_2 of widths w_{in} as they propagate through waveguides with propagation speeds s_1 and s_2 , where we define $s_1 = s_2/2$. Solving for the overlapping region $R = w_{\text{in}} - (s_2 - s_1)t$, we see that $R > 0$ for $0 < t < t_f$. Our gain circuit outputs a pulse v_{out} that remains in a logic-high state for $R > 0$. At $t = t_f = w_{\text{in}}/(s_2 - s_1) = 2w_{\text{in}}/s_2$, the pulse v_{out} , which travels at speed s_2 , has a final width $w_{\text{out}} = s_2 t_f$. Substituting for t_f , we see that $w_{\text{out}} = g(w_{\text{in}}) = 2w_{\text{in}}$. Unfortunately, detectors must be placed at discrete locations x_i along the waveguides to monitor R , which discretizes this gain. However, with minimum separation $\Delta x = x_{i+1} - x_i \ll w_{\text{in,min}}$, the pulse-width gain ~ 2 .

In our circuit, rather than using two waveguides with different pulse propagation speeds, we use a single waveguide (delay line) with detectors placed at specific locations. As shown in Fig. 4b, a single pulse v propagates down a waveguide with speed s where two sets of detectors are placed uniformly at locations $k\Delta x$ and $2k\Delta x$ such that the pulse reaches each set of detectors at times $t = k\Delta x/s$ and $t = 2k\Delta x/s$, respectively. In Fig. 4c, the outputs and overlaps from the detector pairings at $(k\Delta x, 2k\Delta x)$ are shown and the resulting $w_{\text{out}} \sim 2w_{\text{in}}$. By appropriately spacing and comparing detectors, we effectively realize variable pulse-propagation speeds s and

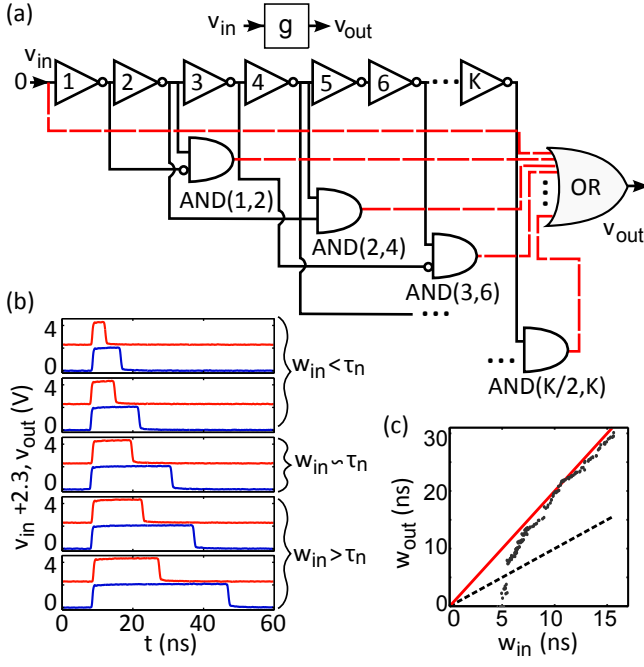


FIG. 3. Pulse-width gain circuit. (a) g with (v_{in}, v_{out}) , $K = 200$ NOT gates, and $K/2$ AND gates that drive a $K/2$ -input OR gate, realized by a tree of gates with balanced path-lengths. Odd-numbered AND gates have one input inverted to balance the logic. (b) v_{in} (top) and v_{out} (bottom). (c) w_{out} for w_{in} at 100 ps steps and dashed (solid) line of slope 1 (2).

$s/2$. Thus in Fig. 3a, the AND-gate outputs approximate the overlap of two pulses that propagate through the delay line at different speeds to yield an approximate pulse-width gain of 2, where the effects of the discrete gates on this gain will be discussed later.

Recall, the map operator of this system $M(w_{in})$ is formed by the composite $g(f(w_{in}))$. Delayed feedback iterates the map $w_{i+1} = M(w_i)$, where w_i (w_{i+1}) is the input (output) pulse-width and i is the iteration index. Interestingly, we might approximate the Lyapunov exponent λ by fitting the return map in Fig. 1e using Eq. [1] to find the average slope m . The fit yields $m_{fit} = 1.95 \pm 0.01$ and $\tau_{n,fit} = 11.7 \pm 0.01$ ns, and using these parameters to estimate λ would give $\sim \ln(1.95)/\tau_N$ [5]. However, using a fit of the return map to estimate λ assumes a continuous map. Based on the discrete nature of the pulse-width gain circuit and the visible discontinuities in the return map, we hypothesize that the discreteness of logic gates on the micro-scale plays a role in the macro-scale dynamics, violating this assumption.

To characterize this multi-scale behavior, we calculate a scale-dependent Lyapunov exponent (SDLE) $\lambda(\epsilon)$ [13–15]. We define our SDLE as the divergence of neighboring trajectories, where neighbors (w_i, w_j) satisfy $\epsilon < |w_i - w_j| < \epsilon + \Delta\epsilon$ (we forgo the Boolean distance metric for Lyapunov calculations, which was used previously for high-dimensional Boolean chaotic systems [2]). An ex-

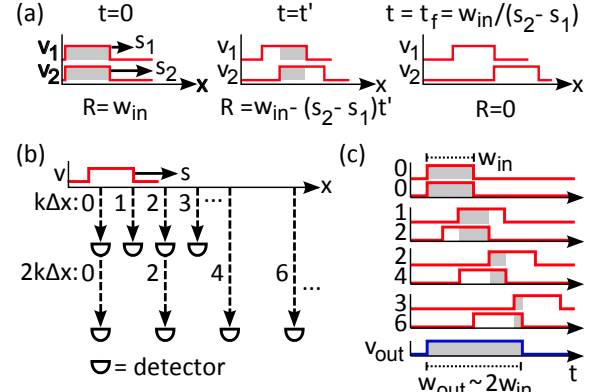


FIG. 4. Pulse-width gain mechanism. (a) Propagations of v_1 and v_2 with speeds s_1 and s_2 at fixed times t . Overlaps are represented as shaded regions. (b) Pulse propagation along a waveguide with detectors at $k\Delta x$ and $2k\Delta x$ for $\Delta x = 1$ and $k = 0$ to $K/2$. (c) Outputs of detectors at $k\Delta x$ and $2k\Delta x$ with overlaps (shaded regions), where $R = 0$ for $k > 3$.

ample of neighboring (w_i, w_j) is shown in Fig. 5a. To calculate $\lambda(\epsilon)$, we average the separation of (w_i, w_j) over neighboring trajectories for a given ϵ . An example is shown in Fig. 5b, where a linear fit of the local divergence shows $\lambda(\epsilon)/\tau_N \sim 0.7$. The calculated $\lambda(\epsilon)$ for a scan of ϵ in 10 ps steps is shown in Fig. 5c. The result decreases rapidly for ϵ in the noise and continues to decrease with oscillations at frequency $\sim 1/(2\tau_1)$ near $\lambda(\epsilon)/\tau_N \sim \ln(2)$, where $\lambda(\epsilon) > 0$ is an indicator of deterministic chaos.

We further investigate this scale dependence using a 1D model for the system's map dynamics. Simulating this map requires a precise model of g , but due to our equipment's resolution, we are unable to measure g on a scale $\sim \tau_1$. As an approximation, we include the effects of the discrete gates and model the pulse-width gain as

$$g(w_{in}) = 2\tau_1 \lfloor w_{in}/\tau_1 \rfloor + h(w_{in} - \tau_1 \lfloor w_{in}/\tau_1 \rfloor), \quad (2)$$

where τ_1 is the average delay through a single gate, $\tau_1 \lfloor w_{in}/\tau_1 \rfloor$ is a measure of w_{in} in gate delays, and h is a function that describes the width of an output pulse for a single gate. As w_{in} increases in Eq. [2], g is discontinuous and increases by steps of τ_1 . We define $h(0) = 0$ such that, when w_{in} is an integer multiple of τ_1 ($w_{in} - \tau_1 \lfloor w_{in}/\tau_1 \rfloor = 0$), the pulse-width gain is exactly 2. When w_{in} is not an integer multiple of τ_1 , h provides a corrective term that describes the continuous growth of pulse widths, where the input to h resets at each multiple of τ_1 . Thus in this model, g is discontinuous with average slope ~ 2 and local slope(s) $h'(w_{in})$.

For simplicity, we let $h(w_{in}) = w_{in}$ and simulate the folding function f in Eq. [1] for $m = 1$ and Eq. [2] in the map $w_{i+1} = M(w_i) = g(f(w_i))$. This model exhibits noise-induced chaos, where it is in a periodic or stable state without the presence of noise [13]. Noise induced-chaos has been previously reported in numerical maps

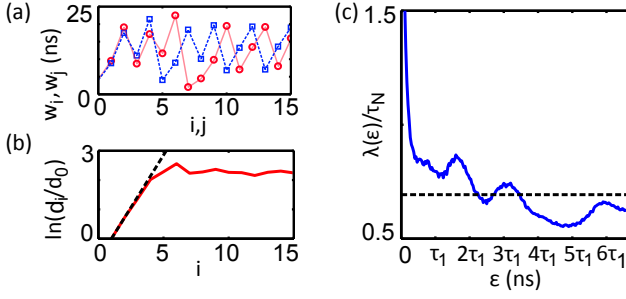


FIG. 5. (a) Neighboring (w_i = dashed line, w_j = solid line) that diverge after several iterations. (b) Average distances $\ln(d_i/d_0)$, where $d_0 = |w_j - w_k|$ for $j \neq k$ and $\epsilon < d_0 < \epsilon + \Delta\epsilon$ for $\epsilon = 700$ ps and $\Delta\epsilon = 5$ ps, with fitted line of slope $\sim \ln(2)$. (c) $\lambda(\epsilon)/\tau_N$ with a dashed line to indicate $\lambda(\epsilon)/\tau_N = \ln(2)$.

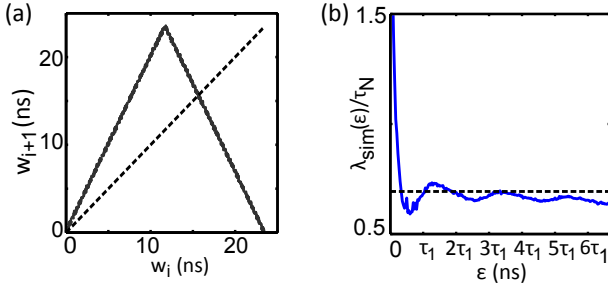


FIG. 6. Numerical simulations of the map $w_{i+1} = M(w_i) = f(g(w_i))$ for $i = 1$ to 4000 using $h(w_{\text{in}}) = w_{\text{in}}$ with noise. (a) Simulated return map (w_i, w_{i+1}) and (b) simulated $\lambda_{\text{sim}}(\epsilon)$ for $\Delta\epsilon = 50$ ps with a dashed line to indicate $\lambda_{\text{sim}}/\tau_N = \ln(2)$.

with fine-scaled discontinuities, where the chaos follows a global map structure [14]. Noise in our experimental system causes jitter in w_i , where the jitter is approximately Gaussian with standard deviation (STD) $\sigma \sim 90$ ps. Thus, we simulate $w_{i+1} = M(w_i)$ with additive-white-Gaussian-noise at every iteration (STD = σ).

The simulated return map is shown in Fig. 6a with a 1D structure similar to a tent map with average slopes $\sim \pm 2$. We calculate the simulated SDLE $\lambda_{\text{sim}}(\epsilon)$ using the same method applied to the experimental data and the result is plotted in Fig. 6b, showing quantitative similarities to $\lambda(\epsilon)$. Thus, this simple model captures the key features of the experimental dynamics (more complex models with heterogeneities in gate-delays and a nonlinear function for $h(w_{\text{in}})$ may show even more agreement). For now, we merely acknowledge that $\lambda(\epsilon)$ and $\lambda_{\text{sim}}(\epsilon)$ show micro-scale features $\sim O(\tau_1)$ that oscillate about the average macro-scale divergence $\sim \ln(2)$ of their respective maps. A theory of these oscillations and their

scaling will be provided in a subsequent publication.

In summary, we present the first instance of experimental 1D Boolean chaos. To do so, we designed a map operator containing folding and stretching circuits on an FPGA. We showed that adding delayed feedback to this operator allows for the circuit to autonomously iterate its 1D chaotic map. The resulting map has features that are reminiscent of the well-known tent-map [5]. However, upon closer inspection, it is evident that the discrete nature of the logic gates on the FPGA lead to scale-dependent features that warrant further study.

S.D.C acknowledges the financial support of the US Army Aviation and Missile Research Development and Engineering Center and is thankful for discussions with Dr. Ned Corron and Dr. Jonathan Blakely. S.D.C. also thanks Dr. David Rosin his procedures in Ref. [16].

-
- [1] D. Dee and M. Ghil, SIAM J. Appl. Math. **44** (1984).
 - [2] R. Zhang, H. L. D. de S.Cavalcante, Z. Gao, D. J. Gauthier, J. E. S. Socolar, M. M. Adams, and D. P. Lathrop, Phys. Rev. E **80**, 045202 (2009).
 - [3] J. N. Blakely, N. J. Corron, S. D. Pethel, M. T. Stahl, and J. Gao, *New Research Trends in Nonlinear Circuits: Design, Chaotic Phenomena and Applications*, edited by I. Kyprianidis, I. Stouboulos, and C. Volos (Nova Publishers, 2014) Chap. 8: Non-autonomous Boolean chaos in a driven ring oscillator.
 - [4] H. L. D. de S. Cavalcante, D. J. Gauthier, J. E. S. Socolar, and R. Zhang, Phil. Trans. R. Soc. A **368** (2010).
 - [5] S. H. Strogatz, *Nonlinear Dynamics and Chaos* (Persues Book Publishing, LLC, 1994).
 - [6] P. Faure and A. Lesne, International Journal of Bifurcation and Chaos **20**, 1731 (2010).
 - [7] N. J. Balmforth, E. A. Spiegel, and C. Tresser, Phys. Rev. Lett. **72**, 80 (1994).
 - [8] D. P. Rosin, D. Rontani, and D. J. Gauthier, Phys. Rev. E **87**, 040902 (2013).
 - [9] D. P. Rosin, D. Rontani, D. J. Gauthier, and E. Schöll, EPL **100** (2012), 10.1209/0295-5075/100/30003.
 - [10] D. P. Rosin, D. Rontani, D. J. Gauthier, and E. Schöll, Phys. Rev. Lett. **110**, 104102 (2013).
 - [11] D. P. Rosin, D. Rontani, and D. J. Gauthier, Phys. Rev. E **89**, 042907 (2014).
 - [12] D. P. Rosin, D. Rontani, N. D. Haynes, E. Schöll, and D. J. Gauthier, Phys. Rev. E **90**, 030902 (2014).
 - [13] J. B. Gao, S. K. Hwang, and J. M. Liu, Phys. Rev. Lett. **82**, 1132 (1999).
 - [14] M. Cencini, M. Falcioni, E. Olbrich, H. Kantz, and A. Vulpiani, Phys. Rev. E **62**, 427 (2000).
 - [15] J. B. Gao, J. Hu, W. W. Tung, and Y. H. Cao, Phys. Rev. E **74**, 066204 (2006).
 - [16] D. P. Rosin, PhD Thesis, TU Berlin (2014).